Materials Chemistry and Physics 272 (2021) 124986

Contents lists available at ScienceDirect

Materials Chemistry and Physics

journal homepage: www.elsevier.com/locate/matchemphys

Aging of anodic titanium dioxide nanotubes in synthetic greywater: Assessment of stability and retention of photocatalytic activity

C. Farrugia [a], F. Lia [b], E. Zammit [b], A. Rizzo [b], V. Privitera [c], G. Impellizzeri [c], A. Di Mauro [c], M. A. Buccheri [d], G. Rapazzo [d], M. Grech [a], P. Refalo [a], S. Abela [a,*]

[a] Faculty of Engineering, University of Malta, Msida MSD 2080, Malta
[b] Institute of Applied Sciences, Malta College for Science Arts and Technology, Malta
[c] CNR-IMM, Via Santa Sofia 64, 95123, Catania, Italy
[d] Department of Biological, Geological and Environmental Science, University of Catania, Catania, Italy

HIGHLIGHTS

- Anodic nanotubes have been found to be extremely resistant to aging and deactivation following a 12-week aging.
- High photocatalytic activities were retained despite the fouling of the surfaces.
- Sustained antibacterial activities at the end of the aging experiment.
- The inter-tube spaces act as catchment areas where debris can accumulate.
- Nanotube layers obtained by anodic oxidation show promise for long term use in greywater treatment reactors.

ARTICLE INFO

Keywords:
TiO_2 nanotubes
Anodizing
Photocatalytic Greywater treatment
Aging

ABSTRACT

Anodic titanium dioxide (TiO_2) nanotubes were found to be highly active photocatalysts which can be used as templates for further modification in order to tailor their photocatalytic activity for a specific application. These photocatalysts possess a high surface area despite being supported, making them suitable candidates for water treatment as no post process recovery is required.

In this work, three different electrolyte compositions together with different process parameters were used to synthesise nanotube arrays having different morphologies. The mechanical and chemical stability together with their photocatalytic activity was studied following a twelve-week aging regimen. The nanotubular surfaces were exposed to flowing greywater under UV-VIS irradiation to simulate daylight. The mechanical and phase stability of the materials were found to be excellent with no degradation and change in crystalline structure being observed. The different morphologies provided different levels of resistance towards fouling with the nanotubes synthesised in the organic electrolyte being the most resistant surface. This resistance to fouling also resulted in the photocatalytic activity being sustained despite the forceful aging conditions. Overall, all the nanotube morphologies were stable making anodizing a suitable synthetic strategy to produce surfaces for real-life applications.

1. Introduction

Honda and Fujishima successfully used a TiO_2 electrode to split water by photoelectrolysis [1]. Their seminal work, spearheaded research into the properties of TiO_2 which had long been used as a brilliant white pigment. This research was targeted mainly to nanoparticles of TiO_2 given that their properties at the nanometric scale are vastly different to those of bulk TiO_2. When exposed to UV light in an environment which contains oxygen, these materials can sustain photooxidative and photoreductive reactions. Such reactions are examples of photocatalysis and can be exploited for the degradation of pollutants both in air and water [2]. This gained insight has led to the widespread use of TiO_2 most notably self-cleaning glass. TiO_2 nanopowders have also been considered as viable candidates for water

* Corresponding author.
E-mail addresses: clayton.farrugia@um.edu.mt (C. Farrugia), stephen.abela@um.edu.mt (S. Abela).

https://doi.org/10.1016/j.matchemphys.2021.124986
Received 9 October 2020; Received in revised form 19 May 2021; Accepted 10 July 2021
Available online 15 July 2021

purification by virtue of their high surface areas which promote high photocatalytic activities. Despite the advantages of their high activity, low-cost and stability, separation of these particles from the treated water is extremely laborious and recovery can never be complete [3,4]. The release of nanoparticles into the environment can have a deleterious effect including their bioaccumulation in the flora and fauna [5,6]. The deposition or binding of the photocatalysts to a substrate like the previously mentioned self-cleaning surfaces can help alleviate the problem of the leaching nanoparticles. This approach is however not without its limitations and release of TiO_2 nanoparticles from paints has been reported by Kaegi [7] and Kattan [8] amongst others. Reijnders has also been critical of researchers labelling nanocomposites containing semiconductor particles as being eco-friendly or non-toxic [9]. Whilst a structurally sound nanostructure can be considered as safe, degradation will always set in to some extent resulting in the release of nanoparticles.

TiO_2 nanotube arrays obtained by anodic oxidation of titanium are self-ordered supported photocatalysts, where the substrate is used as the medium from which they are synthesised. Even though nanotubes and similar nanostructured morphologies can be produced by sol-gel and hydrothermal methods amongst others, these photocatalysts need to be bound to a substrate. Anodic oxidation provides a facile method where nanotubes with a length of several microns can be produced without the need of further processes for deposition. Albeit being superior in that they are found ready bound to a stable substrate; their stability still needs to be assessed. Titanium dioxide is regarded as highly insoluble and free from the effects of photocorrosion after undergoing several cycles of photooxidation and reduction reactions [10]. The anodic nanotubes are however a highly stressed structure with different regions along the tubes being under either tensile or compressive stresses. These stresses are sometimes relieved without any significant outside manipulation resulting in the detachment of the nanotube layer from the substrate [11]. Factors which lead to delamination include drying of the as-produced nanotubes under forced convection and washing the nanotubes after removal from the electrolyte [12]. To address delamination of the as-produced samples, strategies such as the formation of a base compact layer and a secondary anodisation step at lower voltage have been devised [13,14]. Once a stable nanotubular structure is established, the long-term stability during use must be determined. This is imperative in order to guarantee the successful implementation of this technology for water treatment.

Only a handful of studies on the stability and photocatalytic activity of thin coatings have been carried out and these feature materials produced by chemical vapour deposition and sol-gel methods. The stability of such coatings and their activity under flow, immersion and flow/UV exposure regimes has been assessed [15,16]. Both articles report the release of titanium dioxide in nanometric form, despite the inherent stability of both TiO_2 and the binder keeping the TiO_2 immobilised. Even in the case of the homogenous sol gel coating developed by Yao et al. on washing, the photocatalyst coatings lost some of their activity, which the authors attributed to the release of TiO_2. Olabarietta et al. reported the influence of flow induced mechanical damage was extremely low. A much higher release of TiO_2 was however recorded when sodium chloride was added to the aging solution [16].

On the other hand, the stability of anodic TiO_2 nanotubes has been scantly addressed in research works. Changes to the morphology and crystalline structure of non-annealed nanotubes after immersion in aqueous media were reported, however no such work was carried out on annealed nanotubes [17,18]. At the time of writing, the authors have not found reports describing the long-term stability and photocatalytic activity of anodic titania nanotubes in conditions simulating field use. Given that the photocatalytic activity of thermally annealed titania nanotubes exceeds that obtained using other annealing techniques, the viability of these materials should be assessed [19].

In this work, three different nanotube morphologies obtained using different electrolytes were synthesised and aged. The aqueous electrolytes were chosen due to their low cost whilst producing a well-defined nanotubular structure. The experimental parameters for the synthesis using the ethylene glycol were selected to ensure the formation and retention of an oxide layer between the single tubes. The presence of an oxide layer should limit the number of potential sites where debris can accumulate. The seminal work of Assefpour-Dezfuly described the formation of a nanotubular morphology by anodic oxidation in a chromium oxide/ammonium fluoride electrolyte [20]. This work was expanded on by Zwilling, whose own contributions have led to anodic TiO_2 nanotubes being the subject of continued research spanning two decades [21]. The facile method together with an excellent process control make this synthetic strategy highly attractive. The potential of these materials as photocatalysts was described by Macak and the nanotubular arrangements have since been used extensively as templates for further modification [22]. Strategies for enhancing the activity of the semiconductors include doping, decorating with transition metal nanoparticles and dye sensitisation [23–26]. The first syntheses involved the use of aqueous baths containing a mixture of hydrofluoric acid and another inorganic acid [21,27,28]. Subsequent research introduced the use of organic media which led to the synthesis of the most active TiO_2 nanotubular structures [29–31]. The organic electrolytes are however significantly more expensive than their aqueous counterparts. The cost for anodizing of titanium is significant if this technology is to be implemented in water treatment units for consumer use.

Samples representing each morphology were exposed to synthetic greywater containing both chemical and bacteriological components flowing over the surfaces. A UV-VIS light source representing daylight was used to provide 12 h of illumination per day, for twelve weeks. This set-up exposed the materials to the possible effects of mechanical damage to the nanotubes, detachment of the layer, fouling and loss of photocatalytic activity by repeated activations. The effect of this exposure on the changes in morphology, chemical composition and crystalline structure of the materials were monitored by scanning electron microscopy (SEM) imaging coupled with electron dispersive spectroscopy (EDS) and x-ray diffraction (XRD) respectively. The solar absorptance of the materials was calculated from diffuse reflectance values and its variation with aging recorded. TiO_2 being a wide band gap semiconductor (~3.0–3.2 eV), UV light is required for the generation of the charge carrier pair [32]. The solar spectrum contains about 5% UV and thus its absorptance values in this range of wavelengths can help determine the suitability of the materials for solar photocatalytic applications [33]. The use of solar radiation to help bolster photocatalysis' position as an effective green technology is still a thriving research area [34,35]. The changes in photocatalytic activity were assessed by measuring the efficiency in degrading methylene blue (MB) and the antibacterial activity towards *E.Coli*.

The stability of different morphologies obtained using different electrolytes towards exposure to greywater can determine the suitability of these facile, scalable, and effective synthesis methodologies. By identifying the most stable material, the possibility of using anodic nanotubes in greywater treatment solutions is cemented further. A highly stable material can aid in significantly offsetting the production cost thus increasing its cost effectiveness.

2. Experimental

The suitability of the materials for long term use in photocatalytic greywater treatment was assessed by designing a flume on which the materials were exposed to flowing synthetic greywater and UV-VIS light. The synthetic strategies and the characterisation exercises conducted are discussed in the section. The methods by which the photocatalytic activity of both unaged and aged materials is assessed are reported. The design and the rationale behind the aging exercise are described in detail.

2.1. Synthesis of materials

The nanotube arrays were produced by anodic oxidation (anodizing) of commercially pure (99.6%) titanium (Grandis) in a two-electrode set-up. The electrodes were composed of equally sized titanium plates separated by a distance of 30 mm. Prior to the process, the electrodes were sonicated sequentially for 10 min in acetone, followed by isopropanol with a final sonication in deionised (DI) water. The anodizing potential was supplied by a Delta Elektronika SM66-AR-110 power supply and the processes were carried out under potentiostatic conditions. An electrolyte consisting of 3 wt% deionised (DI) water, 0.5 wt% ammonium fluoride (Sigma Aldrich) and ethylene glycol (Scharlau) as balance was used. A potential of 70 V was applied for 1 h and the resulting TiO_2 nanotube array termed TiO_2NT-EG. For the anodizing of titanium in the aqueous media a lower potential was applied as higher potentials result in the loss of the nanostructure. A potential of 20 V was applied for both cases. For the first aqueous bath, an acidic electrolyte composed of a solution of 0.5 wt% sodium fluoride (Sigma Aldich) in 1 M phosphoric acid (Scharlau) was used. The process was conducted for 3 h and the resulting material will be hereafter referred to as TiO_2NT-PA. In the second aqueous bath, a 0.5 wt% sodium fluoride solution in 1 M sodium sulfate (Sigma Aldrich) was the electrolyte employed. In this case the arrays produced are termed TiO_2NT-SS. The anodizing in the last bath required 6 h of processing. For all cases, the as produced nanotubes were gently rinsed with acetone in order to remove the electrolyte following anodizing. The nanotube arrays were then annealed at 450 °C for 2 h. The annealed samples were sonicated for 5 min in isopropanol and air dried.

2.2. Aging of the nanomaterials

The simulated greywater used in this investigation was based on the findings reported by Thompson et al. [36]. Real greywater was used to spike the chemical component of the synthetic greywater with bacteria, diluting 1 part of greywater with 19 parts of the chemical mixture. The greywater was collected from the capture tank of the MCAST greywater treatment facility which collects greywater from the wash hand basins in one of the buildings prior to this being treated. The chemical and bacteriological parameters of the greywater are presented in Table 1. Forty litres of synthetic greywater were circulated over a glass flume with an elevation of 6° where six sets of three 25 × 25mm samples of each material were attached. The synthetic greywater was maintained at 30 °C and flowed over the sample surfaces at a rate of 144 l/h. The flow rate was such that the sample surfaces were flooded in 3 mm of water at all times during aging. Two 26 W Exoterra UVB-100 bulbs together with two 25 W Exoterra Natural Light bulbs served as the light source used to mimic daylight. The bulbs were mounted 9 cm above the sample surface. The calculated UV component of the irradiance over the 18 coupons was found to be between 10 and 12 W/m^2. A 24-h aging cycle comprising 12 h of illumination followed by 12 h in the dark was employed. The duration of the aging regimen was of 12 weeks with sampling intervals set at 1, 4, 6, 8 and 12 weeks where a set of three samples was removed at the end of each interval. A separate tank was used for each material, keeping all experimental parameters identical. The tanks were cleaned weekly together with a replacement of the synthetic greywater. This water change functioned to accelerate the degradation rate of the material, as fresh pollutants were added each week, not allowing any of the single components to be wholly depleted. The low angle of elevation of the flume ensured a better contact of the greywater with the samples. After removal, the samples were gently swabbed with a piece of cotton wool and soaked thrice in isopropanol for 10 min followed by three 1-h soaking cycles in DI water and the samples air dried. A schematic of the aging set-up is provided in Fig. 1.

Table 1
Chemical and bacteriological composition of final greywater mixture.

Chemical or Biological Parameter	Concentration
Cl^-	640.00 mg/L
Ca Hardness	225.00 mg/L
Total Hardness	380.00 mg/L
NO_3^-	17.40 mg/L
NO_2^-	2.60 mg/L
NH_3	4.67 mg/L
Total Phosphorus	0.43 mg/L
Total Surfactants	1.14 mg/L
Total Coliforms	10285.5 ± 3322.5 CFU/mL
E.Coli	855.5 ± 610.7 CFU/mL

2.3. Characterisation

The unaged nanotubes together with the samples aged for predetermined time periods were imaged using a Zeiss Merlin Field Emission Scanning Electron Microscope. For the probe, a voltage of 15 kV and a current of 1 nA were used. Prior to imaging, the aged samples were soaked in deionised water for 10 min to remove any adherent material. This process was repeated twice more and the samples dried using nitrogen. The chemical composition of the active surface was determined with an Apollo EDAX EDS detector mounted on the electron microscope. An area of 1 × 1μm was scanned with an exposure of 100 live seconds. Diffractograms of all the materials during the various stages of the aging experiment were obtained using a Rigaku Ultima IV Cu-Source X-ray Diffractometer. A step size of 0.02 s with a dwell time of 1 s was used spanning from 20° to 90°.

2.4. Spectral absorptance

Diffuse reflectance spectra were obtained using a Shimadzu SolidSpec-3700 UV-VIS spectrometer housing an integrating sphere. The spectra were obtained at 1 nm increments at medium speed over the range between 280 and 700 nm. The absorptance values were corrected to account for solar global tilt as described in ASTM G173-03 standard [37]. The total spectral absorptance was calculated using equation (1).

$$\alpha = \frac{\int_{\lambda_1}^{\lambda_2} \alpha_\lambda G_\lambda d_\lambda}{\int_{\lambda_1}^{\lambda_2} \alpha_\lambda d_\lambda} \quad (1)$$

Where λ is the wavelength α_λ is the absorptance at a specific wavelength, G_λ is the spectral irradiance at a specific wavelength.

2.5. Quantification of photocatalytic activity

A more holistic assessment of the photocatalytic activity can be found in our previous work [38]. In this previous publication, the effect of pH on activity and the different reactive oxygen species (ROS) involved in the degradation reactions were quantified and identified. The microorganisms which are more susceptible to photocatalytic disinfection were also identified. In this work, a facile protocol for assessing the changes in photocatalytic activity was developed. The method described in ISO 10678:2010 was adopted to quantify the photocatalytic activity [39]. The volume of the MB solution was reduced to 10 mL whilst the other variables described in the standard were left unchanged. The samples were initially irradiated for 1 h at a wavelength of 365 nm and an intensity of 1.2 mW/cm^2 using an Opsytec BS-02 chamber with a UV MAT controller. This removed any adventitious hydrocarbons from the surface [40]. The samples were immersed in 10 mL of a 1.5 × 10^{-5} M methylene blue solution and allowed to reach the absorption-desorption equilibrium for 1-h in the dark. The absorbance of the solution after irradiation was measured at 30-min intervals over a period of 4 h. A scan range between 500 and 800 nm was used to read the absorbance maximum at 664 nm on a Shimadzu SolidSpec 3700i.

A culture of *Escherichia coli* ATCC® 8739™ was incubated with shaking at 37 °C at 120 RPM under aerobic conditions for 8 h. The

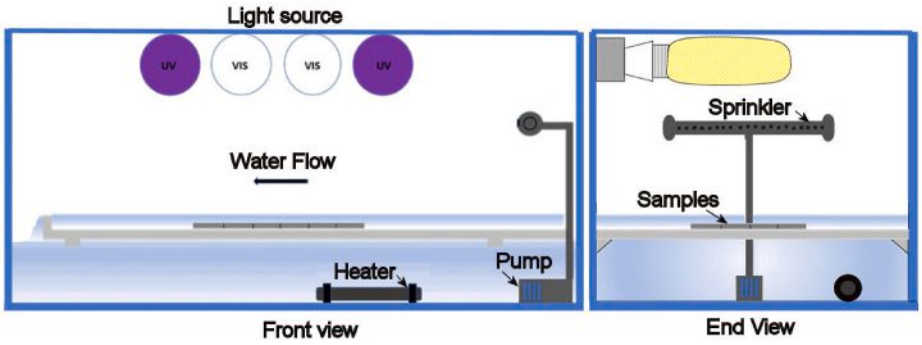

Fig. 1. Schematic showing the main components of the aging module.

optical density of the culture was adjusted with tryptic soy broth to 0.5 abs units at 600 nm equivalent to 1.5×10^8 CFU. A 200 μL aliquot of the prepared microbial solution was spread uniformly over the sample surface using a micropipette and placed in a climatic chamber (ICH 256 Memmert GmbH) held at 37 °C and 80% relative humidity. The aged samples and a titanium metal blank were placed on a glass microscope slide place over a 5 cm open petri dish. To the petri dish 10 mL of water were added to prevent the bacterial solution from drying out. After 1 h of irradiation the coupon was transferred into a sterile 5 cm petri dish and 1 mL of sterile phosphate buffered saline (PBS) was added. The petri dish was gently shaken to recover all the bacterial solution. The PBS solution was transferred into a sterile Eppendorf tube and from which aliquots were taken to prepare a serial dilution with a range of 10^2 to 10^6. A 50 μL aliquot from each dilution was plated onto total count agar and incubated upside down for 10 h at 35 °C. The number of colonies cultured were counted and the photocatalytic activity with respect to a titanium blank was calculated.

3. Results and discussion

The morphology of the surfaces was assessed for signs of delamination, photocorrosion and flow assisted degradation. Possible changes to the crystalline structure and chemical composition of the surfaces were similarly investigated. The photocatalytic activity after the aging experiment was determined and corroborated to the physical and chemical changes recorded.

3.1. Morphology and chemical composition

On analysis of the SEM images of the aged surfaces the reduction in exposed surface area due to the build-up of debris was immediately noticeable. The percentage exposed area of the array has been estimated by image analysis of the SEM images of aged surfaces imaged at 20 K magnification (not shown here). The trend with time is plotted in Fig. 2. This magnification was found to make quantification easier. The percentage exposed area for TiO_2NT-EG decreases gradually with each aging time point, reaching a final value of 86%. For TiO_2NT-PA, the coverage until the fourth week of aging was relatively low, with around 89% of the surface being free from debris. However, by the sixth week, only 4% of surface was not fouled, eventually reaching a value of 2% by the twelfth aging interval. On the TiO_2NT-SS surface a large decrease in the exposed area is recorded after just four weeks of aging, where the value decreases to 61%. This is followed by a further small decrease after six weeks. Less than half of the surface was exposed by the eighth week. The final value at 27% was extremely low when compared to the final value for TiO_2NT-EG however the exposed surface area was significantly higher than that of TiO_2NT-PA. The remainder of this section discusses the morphology of the different materials in more detail.

Image analysis of the array surfaces and their cross section was used to determine the tube diameters and array thicknesses. The average tube

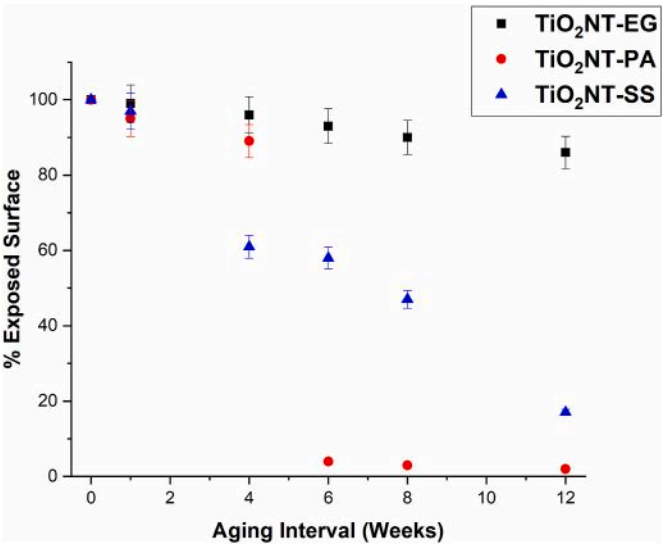

Fig. 2. Variation in percentage exposed surface along the aging timeframe.

diameter for TiO_2NT-EG was around 80 nm and the layer thickness 10 μm. The TiO_2NT-PA arrays were considerably thinner at 700 nm with their average tube diameter being about 105 nm. In terms of layer thickness, TiO_2NT-SS at 1.6 μm was nearly twice as thick as TiO_2NT-PA but significantly thinner TiO_2NT-EG. The average tube diameter was around 65 nm.

The surface morphologies of TiO_2NT-EG arrays during the different stages of the aging exercise are presented in Fig. 3a to f. The unaged array in Fig. 3a shows that the individual nanotubes in TiO_2NT-EG appear to be fused to their neighbouring tubes with no inter-tube spaces visible on the surface. This fused appearance is due to remnants of the compact oxide layer formed during the initial stages of the anodizing. This layer is etched by the field assisted migration of the fluoride ions which leads to the formation of the nanotube morphology [41]. Discrete nanotubes were still produced despite the fused appearance, and these can be seen in Fig. 4 which presents a cross section view of the arrays after the fourth week of aging. This oxide layer was not removed as it could serve as a barrier against entrapment of debris in the inter-tube spaces, possibly enhancing the fouling resistance of the material. The outer diameter of the tubes whilst not very well defined, is noticeable, indicating the formation of nanotubes rather than nanopores. A more complete etching of the nanotubes could have been achieved by applying the potential for longer. Similarly, ultrasonication can help detach this oxide layer holding the nanotubes together. The surface morphology of the nanotubes in TiO_2NT-EG was mostly unchanged after one week of aging (Fig. 3b). Supplementary Fig. 1B reveals no dissolution or perforation along the length of the nanotubes. Also, there was no

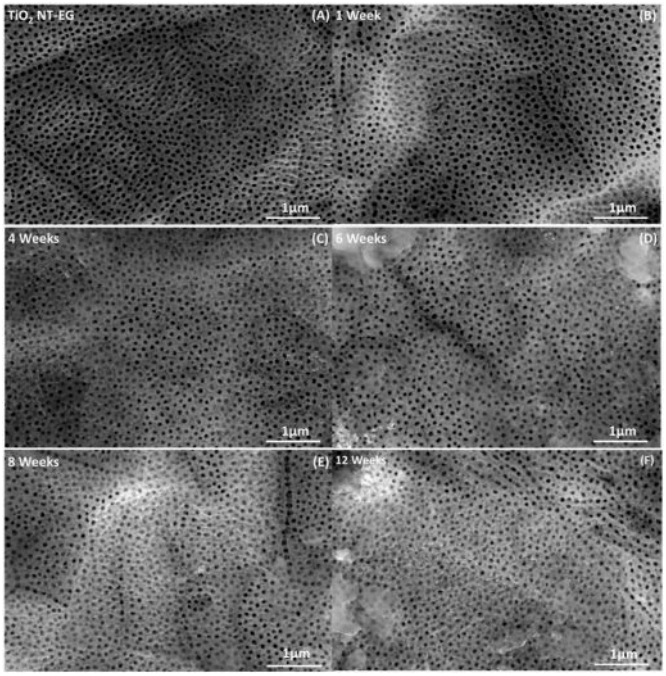

Fig. 3. Morphological changes on TiO2NT-EG Surface: a) Unaged b) Week 1 c) Week 4 d) Week 6 e) Week 8 f) Week 12.

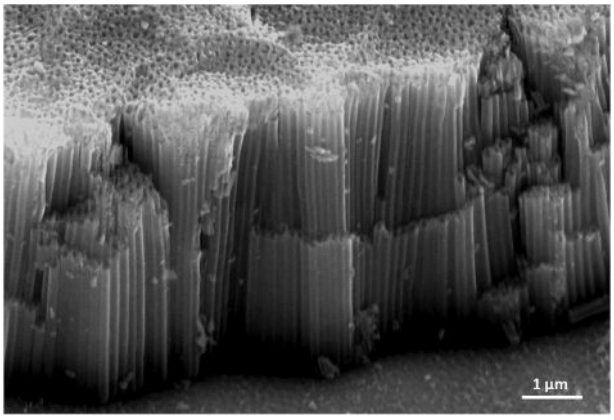

Fig. 4. Cross-section SEM image showing the morphology of the discrete nanotubes after 4 weeks of aging.

evident structural damage to the nanotubes from the top, and the nanotube layer was still adherent to the substrate. The presence of a fluoride rich layer at the nanotube bottom-substrate interface has been reported by Yu [13] and Habazaki [42] where they report that its dissolution can result in delamination of the nanotube layer. Similarly, Berger et al. have reported that fluoride rich areas can be found to be present along the inside of the nanotubes and in the inter-tube spaces [43]. In this study, the as-produced nanotubes were rinsed in acetone to avoid dissolution of the fluoride rich bottom layer to avoid delamination of the layers. The only slight change in the morphology of the surface was that the nanotubes became more defined and the single nanotubes could be discerned. This might be due to the fluoride induced etching or the removal of loosely bound TiO_2 particles by the flow of water over the surfaces. This cleaning action has been previously reported and was attributed to the combined effect of water flow and the UV irradiation [44]. Supplementary Fig. 1c and Fig. 4 reveal that the integrity of the tubes was retained even after four weeks of aging. However more distinct changes to the nanotube surfaces were recorded as shown in Fig. 3c. The outer diameter of the individual nanotubes is even more well defined than it was after the first week. Accumulation of debris around the tube tops is evident with some of the tubes being occluded by the material. Translucent crystals were also deposited over the surface with the tube tops clearly visible underneath. An approximate chemical composition of the particles was determined by EDX (Fig. 5). The translucent particles are most likely kaolin crystals. Kaolin crystals can have a hexagonal or prismatic flake morphology [45]. The silicon and aluminium content of these shards confirms the identity of the particles, the low values are due to the characteristic radiation originating from the substrate being picked up by the EDS detector, as the shards are extremely thin, thus reducing the overall reported concentration of these elements. When these flake-like shards are packed into a more voluminous shard, the silicon and aluminium contents are much higher. The other elements belong to the salts and the organic compounds making up the synthetic greywater. No changes to the nanotubes along their lengths were recorded for the remaining aging intervals (Supplementary Figs. 1D–F). The condition and the morphology of the surface from the sixth week (Fig. 3d) onwards mostly resembled that recorded in the fourth week albeit with a higher degree of coverage of the surface with debris. The definition of the outer tube diameter was reduced as small particles filled the slight depressions around it and is clear by the eighth week (Fig. 3e). By the end of the twelfth week of aging, the singular nanotubes could not be discerned, however a significant number of tube pores remained open (Fig. 3f). Most importantly, no detachment or breakage of the nanotubes was visible, indicating that the arrays are resistant to mechanical damage by the flowing water, continued fluoride assisted etching and photoinduced corrosion. The likely inclusion of carbon within the nanostructure when ethylene glycol was used does not appear to have any detrimental effect on the stability of the arrays. Despite the weekly loading with more solid particles, the nanotubular morphology was found to be resistant to extreme fouling. The relatively narrow nanotube diameter at around 80 nm, coupled with the absence of spaces between the tubes made accumulation of material on the surface more difficult.

The surface morphology of the unaged TiO_2NT-PA nanotubes is presented in Fig. 6a. Cross section images for both materials synthesised in the aqueous electrolyte could not be obtained as their low thickness resulted in excessive damage when the samples were prepared for imaging. The nanotubes are very well structured and significant inter-tube spaces exist around each tube. After one week, the inter-tube spaces proved to be the sites where accumulation of debris was the most severe (Fig. 6b). A compact continuous layer of debris can be seen at the four corners in this figure with the upper and bottom right-hand corner being the more conspicuous. The morphology of this debris layer can be seen in more detail in Supplementary Fig. 2. The inter-tube spaces were nearly all filled by the end of the fourth week and the surface was extensively covered with debris (Fig. 6c). The composition of this material is close to that observed on the TiO_2NT-EG surface with the composition at two locations being recorded in Fig. 7. The surface at the end of the sixth week shown in Fig. 6d resembled that of week four. The coverage with the compact and consolidated layer was extensive, with the debris pervading both the nanotube openings and the inter-tube spaces. This trend of material accumulation continued into the eighth (Fig. 6e) and twelfth week (Fig. 6f), with the debris forming mounds over the previously deposited compact layers. The spacing between the tubes combined with a larger nanotube diameter of around 105 nm greatly facilitated the build-up of debris. One other noticeable change from the TiO_2NT-EG surface is the development of dark areas which can be clearly seen in Fig. 6e and f. This has been attributed by Fischer to be due to fouling by organic species [46]. Despite the ability of the materials to degrade organic matter, the weekly addition of cellulose and bacteria and other complex organic compounds could limit the efficiency of the surface. This loss in efficiency can be derived from the coverage and subsequent shadowing of the surface by insoluble material.

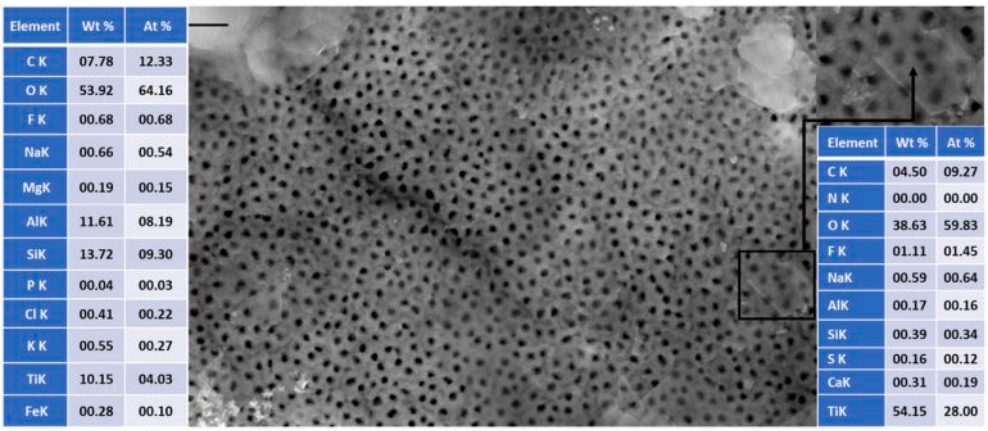

Fig. 5. Chemical constituents of translucent quasi-hexagonal particles on the surface of the TiO2NT-EG array aged for six weeks.

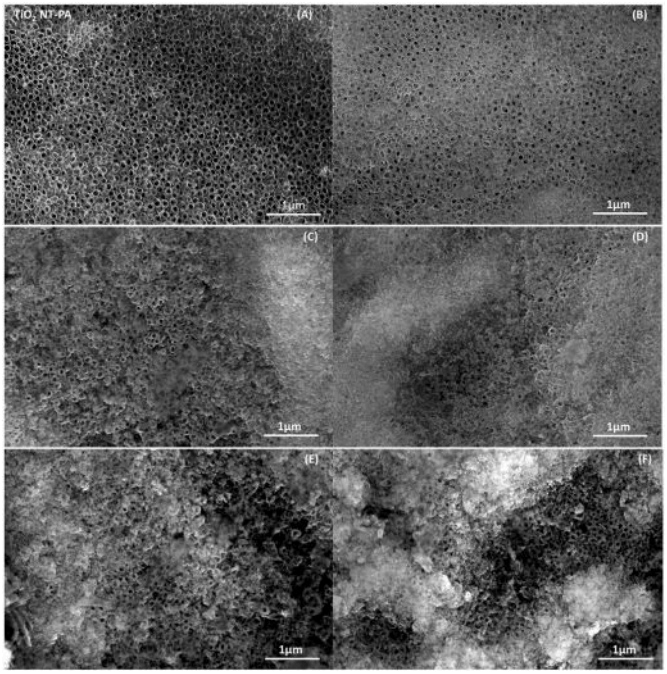

Fig. 6. Morphological changed on TiO_2NT-PA Surface: a) Unaged b) Week 1 c) Week 4 d) Week 6 e) Week 8 f) Week 12.

The unaged TiO_2NT-SS surface shown in Fig. 8a, is less uniform than that of TiO_2NT-PA. The tubes within the TiO_2NT-PA array, at 700 nm, are about half as long as those belonging to TiO_2NT-SS. The lengths of the individual TiO_2NT-SS nanotubes are less consistent, with the shorter nanotubes appearing as recessed areas. The inter-tube spaces are also less well defined. Tubes with more erratic shapes and narrower diameters are nested in the voids formed between the tubes having a larger diameter. The nanotube tops of TiO_2NT-SS show very little occlusion after one week which is confined to the top right-hand corner of Fig. 8b. The 65 nm wide tubes reduced the ability of the solids to penetrate the nanostructure. The nanotubes in the recessed areas appear to not have been appreciably affected, with the debris being caught by the longer nanotubes. This lower occlusion rate was somewhat retained up to the fourth week (Fig. 8c). A compact layer like that observed for TiO_2NT-PA was eventually formed and can most clearly be seen on the left-hand portion of the micrograph. Prismatic particles are also found on the surface, but these are thicker than the ones reported in Fig. 3. More unobstructed nanotube tops were present than on the TiO_2NT-PA surface at the same aging time interval. The number of occluded nanotubes was however much higher than that found on TiO_2NT-EG. Despite the increase in deposited material, a significant portion of the surface was still uncovered after six weeks of the aging regimen with unobstructed tube tops were still visible (Fig. 8d). The accumulation of debris continued over the eighth and twelfth week as presented in Fig. 8e and f respectively, however rather remarkably, the surface was still not completely occluded.

3.2. Changes in crystalline structure

The crystalline phases present on the aged coupons are presented in Fig. 9. The crystalline composition of TiO_2NT-EG is shown in Fig. 9a, with anatase being the major phase present. An extremely low peak at around the 68.8° 2θ value can be attributed to the rutile phase. This phase composition is typical of the annealing procedure employed in this study, with the reported contribution of the rutile phase towards photocatalytic activity being negligible [47,48]. Phase stability has been reported by Cao et al. however, the authors did not expose the material to UV light and/or to solutions with an organic load [18]. Whilst the anatase to rutile transition is unlikely to occur at room temperature, the formation of other phases due to repeated photocatalytic activation needs to be assessed [49]. X-Ray diffraction analysis conducted on samples subjected to the twelve-week aging tests, gave results in which the ratio of the peak heights for both phases remained similar despite anatase being a metastable phase. This result suggests that there has not been any appreciable anatase to rutile transformation in the test samples. Structural changes promoted by photocatalytic activation and the possibility of defects during production of the nanotubes possibly might cause the phase transformation, however this was not recorded [50]. One distinct change was the detection of a peak at 2θ 31.54° already visible after one week of aging. This peak belongs to halite, indicating the presence of sodium chloride onto the surface. Even though sodium chloride is very easily soluble in water and that the samples were rinsed and immersed in DI water, some of the salt layer remained. One explanation for this is that sodium chloride trapped within the nanostructure was solubilised with each cleaning and immersion cycle and on drying this re-deposited onto the surface. The high ionic mobility of Na^+ and Cl^- in solution could have aided the migration of these ions through the nanotubular structure towards the surface [51]. Given that sodium chloride was the most abundant salt in the synthetic greywater, its detection on the surface of the sample, could be simply a matter of quantities.

The XRD profile of the unaged TiO_2NT-PA presented in Fig. 8 resembles that of TiO_2NT-EG (Fig. 8b) in terms of the phases present. Even in the case of TiO_2NT-PA, anatase is the prevalent TiO_2 polymorph produced after annealing. In this case, X-Ray analysis shows the presence of peaks at 2θ 27.46° and 31.60° originating from halite and were

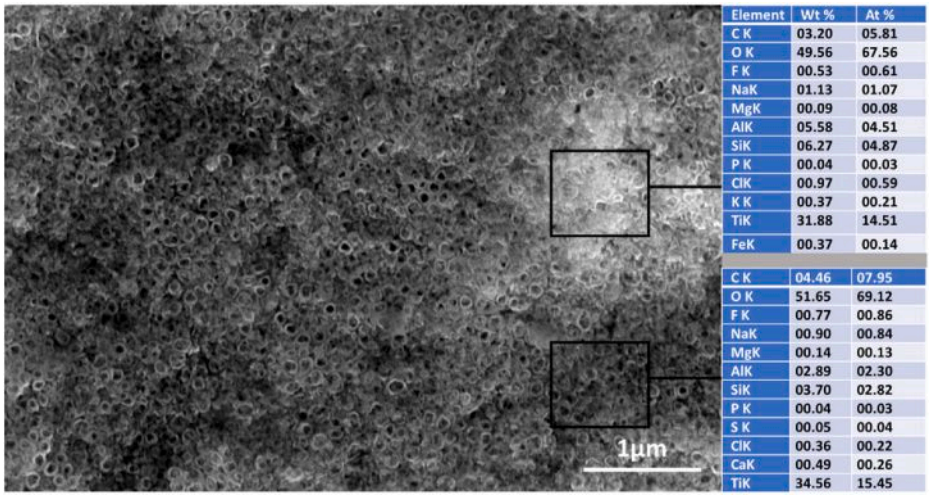

Element	Wt %	At %
C K	03.20	05.81
O K	49.56	67.56
F K	00.53	00.61
NaK	01.13	01.07
MgK	00.09	00.08
AlK	05.58	04.51
SiK	06.27	04.87
P K	00.04	00.03
ClK	00.97	00.59
K K	00.37	00.21
TiK	31.88	14.51
FeK	00.37	00.14
C K	04.46	07.95
O K	51.65	69.12
F K	00.77	00.86
NaK	00.90	00.84
MgK	00.14	00.13
AlK	02.89	02.30
SiK	03.70	02.82
P K	00.04	00.03
S K	00.05	00.04
ClK	00.36	00.22
CaK	00.49	00.26
TiK	34.56	15.45

Fig. 7. Chemical constituents of compacted debris on TiO_2NT-PA Surface aged for 6 weeks.

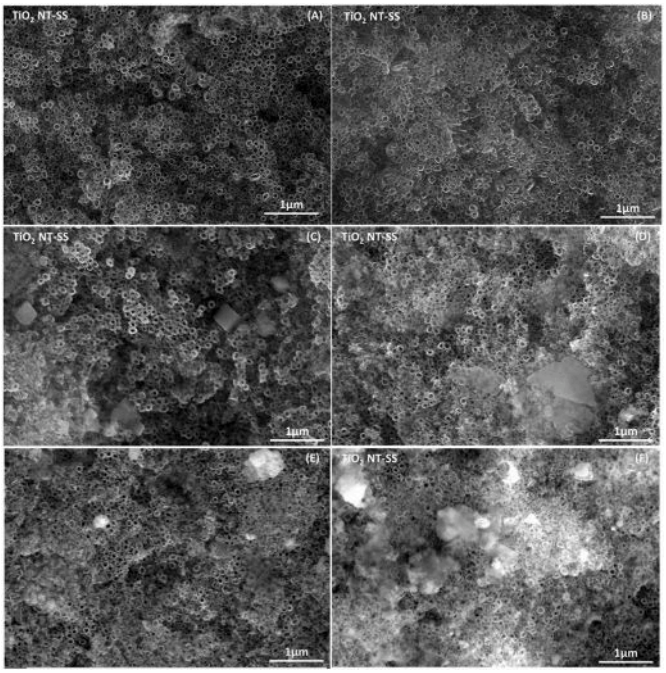

Fig. 8. Morphological changes on TiO2NT-SS Surface: a) Unaged b) Week 1 c) Week 4 d) Week 6 e) Week 8 f) Week 12.

extremely prominent after just one week through the aging regimen. The identity of the particles was verified through EDS analysis of some of the cubic particles present on the surface (Supplementary Fig. 3). The relative intensity of the peaks is highest at the twelfth week time point. This is indicative of the build-up of debris on the surface, which aided in hindering the leaching of the salt during the sequential cleaning steps. If the debris particles were not porous enough or the rate of travel of the salt through the layer was slow, the debris layer could act as concentration sites for sodium chloride and the other soluble salts. The anatase-rutile transformation has also not been recorded for this material at the conclusion of the aging regimen.

The TiO_2NT-SS array contains anatase as its main semiconductor oxide constituent (Fig. 8c). In this case, the peaks at 2θ 27.46° and 31.60° were recorded after the fourth week of exposure, with the peak at 31.60° being particularly prominent. The intensity of the halite peaks did not vary appreciably after the fourth week, which can be corroborated with the relatively unchanged surface recorded for the subsequent aging time points. Even for these samples, the anatase polymorph was also stable, with no rutile being detected up to the end of the experiment.

3.3. Variation in spectral absorption

The spectral absorption traces for TiO_2NT-EG for each aging timepoint are presented in Fig. 10a. An increase in the absorptance of the material in the UV region has been noticed in all the aging instances. This can be attributed to the loss of reflectance of the surface by the coverage of the surface with debris. The top of the nanotube walls can act as a mirror, maximizing the reflected light reaching the UV-VIS sensor [52]. Superior reflectivity has also been attributed to regular, upright morphology of the tubes which limits the loss of light by scattering [52]. The deposition of the debris covered the initially reflective tube tops. The stacking of debris could also have made UV transparent materials such as Kaolin absorb more strongly. The traces for TiO_2NT-PA (Fig. 10b) vary considerably with no discernible shift in the UV region absorption maximum. The deposition of debris has however increased the opacity of the surface, as the oscillations recorded in the visible region were absent after the first week of aging. The oscillations are characteristic of thin transparent films irradiated by low energy light, TiO_2NT-PA being an example of such a thin film [53]. Similarly, to TiO_2NT-EG, an increase in the absorption maximum in the UV region was recorded for TiO_2NT-SS (Fig. 10c). The UV absorptance of the aged materials has increased with respect to that in the as produced state. This is likely due to the absorption of light by the debris. The additional absorbance of UV light especially 365 nm, does not necessarily imply an increased activity with aging. There is no evidence that the energy from the additional photons absorbed is in any way transferred to the nanotubular arrays. The total spectral absorptance for the different arrays was calculated and are collected in Table 2 and presented graphically in Fig. 11.

3.4. Photocatalytic activity: degradation of methylene blue

The effect of different morphologies with respect to organic pollutants including MB is the subject of one of our previous works. In the article we reported the superior activity of TiO_2NT-EG (termed TiO_2NT-O in the published work) and attributed this mainly to the higher thickness of the material produced in the ethylene glycol based electrolyte [54]. The anatase content and tube diameters were also contributing factors but to a lower extent. The activity of TiO_2NT-EG at the different aging timepoints is presented in Fig. 12. The TiO_2NT-EG

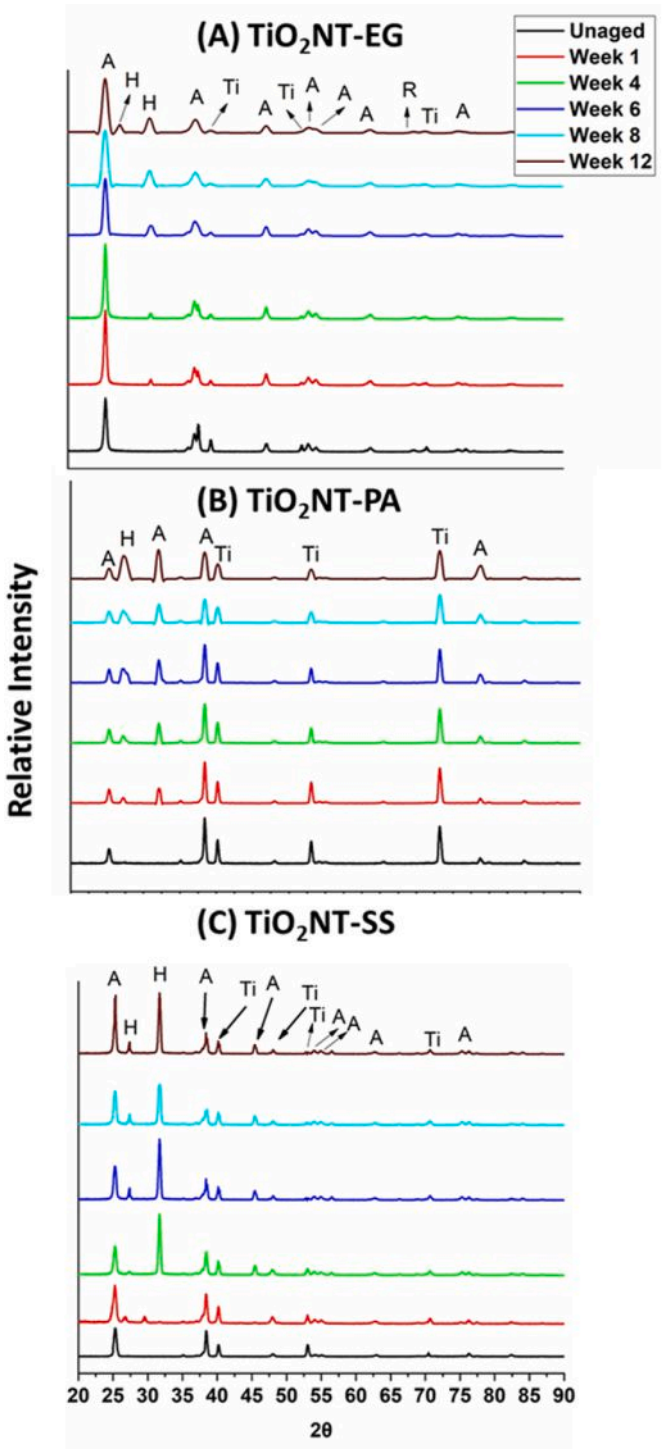

Fig. 9. Changes in crystallographic structure of the nanotube arrays during aging regimen (a) TiO_2NT-EG (b) TiO_2NT-PA (c) TiO_2NT-SS.

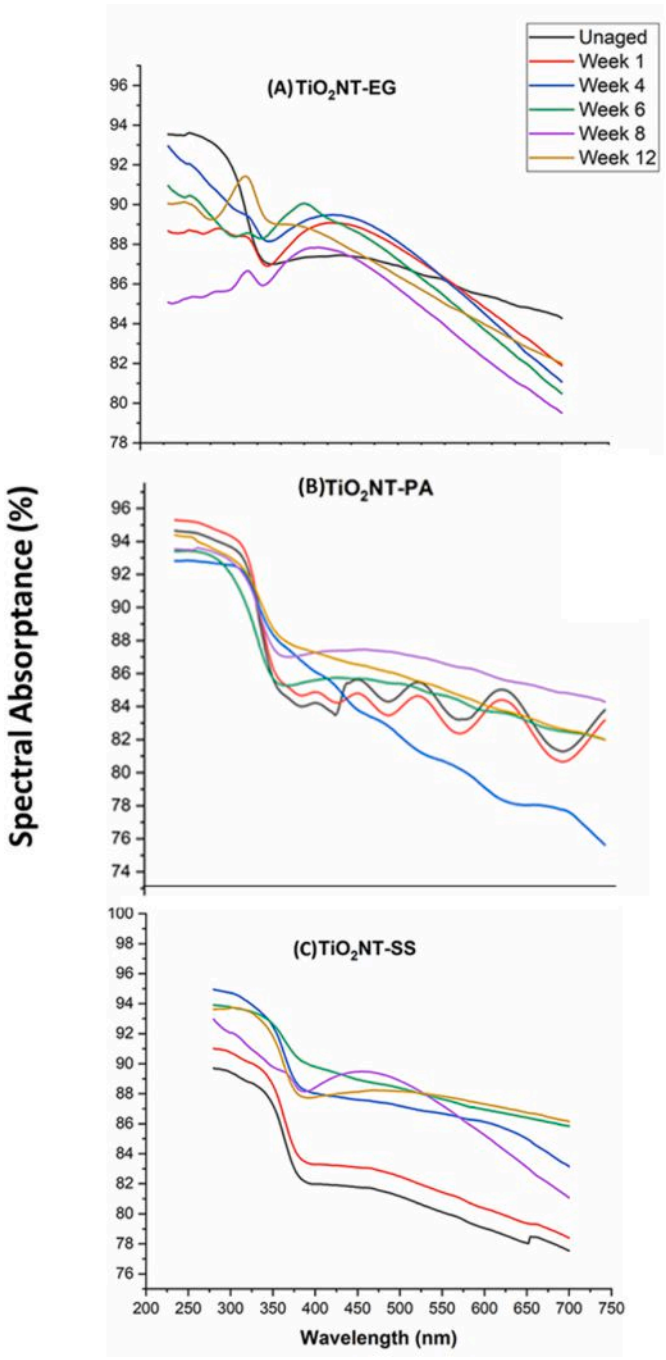

Fig. 10. Changes in spectral absorptance of the nanotube arrays during aging regimen (a) TiO_2NT-EG (b) TiO_2NT-PA (c) TiO_2NT-SS.

array with a rate constant of 0.01425 min^{-1} towards the degradation of methylene blue is the most active of the three active materials investigated. Even though closely packed nanotube layers usually show lower photocatalytic activities due to their lower exposed surface area, this result is not quite unexpected. The regular upright morphology of the TiO_2NT-EG coupled with the significant thickness of the layer ($\approx 10\mu m$) ensures an effective intake of the pollutant within the structure and efficient absorbance of light. In addition, the higher exposed volume of the photocatalyst ensures the production of more electron-hole pairs and electrons at the surface. Despite the appearance of the surface being overall similar to that of the unaged samples, there is a significant reduction in the activity for the aged samples, with the rate constant falling to 0.00646 min^{-1} after just one week of aging. Competitive inhibition mechanisms have been determined to reduce the overall photocatalytic activity [55]. Organic compounds on the surface can scavenge the ROS generated and thus reduce their availability for reaction with the pollutant [56–58]. Similarly, the presence of certain inorganic anions such as phosphate, nitrate, sulfate, and carbonate in solution has been found to lower the overall reaction rate [59–61]. These species can either occupy possible adsorption sites on the surface or scavenge the ROS directly. Guillard has reported the formation of a salt layer on the surface which inhibits the adsorption of methylene blue [62]. All the anions mentioned previously are present in the synthetic

Table 2
Total Spectral absorptance Values (UV (280–400 nm), UV-365nm, VIS (400–700 nm), Total (280–700 nm)).

Material	Spectrum	Unaged	Week 1	Week 4	Week 6	Week 8	Week 12
TiO_2NT-EG	UV	86.1 ± 1.3%	87.9 ± 1.2%	89.3 ± 1.1%	88.7 ± 1.2%	90.2 ± 1.3%	90.0 ± 1.4%
	UV-365	86.7 ± 0.03%	88.5 ± 0.12%	89.5 ± 0.08%	88.6 ± 0.05%	89.2 ± 0.12%	91.4 ± 0.07%
	VIS	84.4 ± 1.2%	86.3 ± 1.5%	86.5 ± 1.2%	85.9 ± 1.1%	87.4 ± 1.3%	85.7 ± 1.1%
	Total	84.6 ± 1.1%	86.7 ± 1.4%	86.8 ± 1.2%	86.1 ± 1.3%	87.7 ± 1.4%	86.1 ± 1.6%
TiO_2NT-PA	UV	88.7 ± 1.0%	89.3 ± 1.2%	89.8 ± 1.1%	88.0 ± 1.1%	89.6 ± 1.4%	90.2 ± 1.2%
	UV-365	84.6 ± 0.08%	89.0 ± 0.07%	89.6 ± 0.05%	87.2 ± 0.09%	89.2 ± 0.06%	90.1 ± 0.10%
	VIS	83.9 ± 1.1%	83.4 ± 1.2%	80.7 ± 1.3%	84.3 ± 1.0%	86.3 ± 1.2%	84.8 ± 1.1%
	Total	84.6 ± 1.2%	84.0 ± 1.3%	81.6 ± 1.4%	84.6 ± 1.2%	86.6 ± 1.1%	85.3 ± 1.3%
TiO_2NT-SS	UV	84.9 ± 1.0%	86.3 ± 1.1%	90.6 ± 1.3%	91.5 ± 1.2%	89.3 ± 1.1%	89.9 ± 1.4%
	UV-365	88.6 ± 0.17%	86.0 ± 0.08%	90.4 ± 0.06%	91.5 ± 0.05%	89.1 ± 0.09%	89.6 ± 0.08%
	VIS	80.0 ± 1.5%	81.3 ± 1.4%	86.4 ± 1.0%	87.7 ± 1.3%	85.3 ± 1.0%	87.6 ± 1.2%
	Total	80.5 ± 1.4%	81.8 ± 1.0%	86.8 ± 1.1%	88.1 ± 1.4%	85.4 ± 1.2%	87.8 ± 1.5%

greywater and they might have leached into the surface structures during aging. Similarly, these anions might have been the components of a thin inorganic film deposited on the surface. The presence of halite on the surface recorded in the diffractograms corroborates the thesis of the formation of an inorganic layer. Rinsing with DI water whilst successful in removing the macroscopic material which adhered to the coupons, might not have been sufficient for the complete leaching of the adsorped species. A further reduction in activity was recorded for the sample extracted after four weeks of exposure with the rate constant dropping to 0.00479 min^{-1}. The significantly abundant particles most likely hindered the approach of the molecules towards the surface, where the molecules might have adsorped preferentially to the particles. Despite the initial stages of fouling, with the first closure of the tube tops occurring, a high level of activity was retained. After the initial reduction in activity recorded in the first four weeks, the activity did not decrease much further with subsequent aging. The values of the rate constant for the sixth, eighth and twelfth weeks were 0.00449 min^{-1}, 0.00452 min^{-1} and 0.00433 min^{-1} respectively. Relatively high activities were retained notwithstanding the weekly water changes, which ensured that the concentration of contaminants in the greywater was practically unchanged. This morphology of this material, did not favour the clogging of the surfaces with debris, leaving an amply exposed surface. The kaolin particles are also transparent to low energy UV, allowing our light source to sufficiently irradiate the surface [45,63].

The temporal variation in activity of TiO_2NT-PA is shown in Fig. 13. The rate constant of the as-produced TiO_2NT-PA array is 0.00715 min^{-1} This is significantly lower than that for the array produced in ethylene glycol despite the higher exposed surface area due to the clearly defined inter-tube spaces, showing that the tube length is more influential than the surface morphology. This array with a thickness of about 700 nm can allow a lower volume of pollutant within its tubes together with having a lower charge carrier production rate. The lower thickness has been attributed to the very fast fluoride mitigated etching when aqueous media are employed. For these samples, a significant reduction in activity was recorded after just one week of testing with rate constant dropping to 0.00436 min^{-1}. It is believed that the occlusion of the nanotubes has reduced the ability of the surface to interact with the dye and with light. Even so, the activity was not completely stifled as the tube tops were still exposed together with several nanotubes not becoming occluded. The reaction rate after one month of aging is 0.00248 min^{-1}. This can be correlated to the copious amounts of tightly adherent debris deposited on the surface. Activity was retained as the surface was not wholly fouled, allowing for the photocatalytic activity to be sustained. A similar trend to that observed for TiO_2NT-EG was also obtained. The degradation rates for the last three timepoints were nearly identical to that obtained after four weeks of aging had elapsed. Given that exposed nanotubes are still present, some level of activity can still be sustained.

Fig. 14 displays the activity of TiO_2NT-SS at each experimental time point. The rate constant of unaged TiO_2NT-SS at 0.00797 min^{-1} is close to that of TiO_2NT-PA, despite the former being nearly twice as thick ($\approx 1.44\mu m$) as the latter. The narrower tubes limit the rate of transport of the dye within the nanostructure. The trend observed for the other two nanotube arrays was also recorded for this material. The greatest loss in activity occurred over the first four weeks of exposure. An initial drop to 0.00566 min^{-1} after the first week was followed by the activity falling to 0.00323 min^{-1}at the end of the fourth week of aging. The available surface was not significantly reduced after one week, but a reduction in activity was still recorded. The further decline in activity mirrors the considerable amount of debris accumulated by the second aging time point. Further significant changes in activity were not recorded. Despite the weekly addition of insoluble material, fouling of the nanotubular structure was not complete. This could have been aided by the smaller nanotube diameters which reduced the entry of particles belonging to a larger size fraction.

The loss in dye degradation efficiency, expressed in terms of the percentage degradation of MB for all three materials, is summarised in Fig. 15. For TiO_2NT-EG the degradation rate declined from 96% for the unaged material to 65% at the end of the aging regime. A drop from 83% to 46% over the 12-week period was recorded for TiO_2NT-PA. A final degradation rate of 51% was obtained for TiO_2NT-SS from the initial 85% of the unaged material.

3.5. Photocatalytic activity: antibacterial activity

Despite sharing many similarities, the mechanisms of degradation of organic molecules and photocatalytic anti-bacterial activity differ on whether contact with the surface is required [64]. Organic molecules must be in direct contact with the surface, where the geometry of the approach and the strength of adsorption to the surface play a significant role in determining the rate of reaction. On the other hand, bacterial inactivation or disinfection mechanisms can be sustained at a distance from the surface. The ROSs produced can migrate within the solution and react with the bacterial cell membrane or diffuse through the cell membrane. Lysis of the cell membrane results in the leakage of ions and proteins from the cell thus disrupting its function. The diffusion of ROS into the bacterial cells can oxidise and thus destroy the structure of DNA.

The degradation rate of bacteria is closely related to the activity of the material towards other types of photocatalyzed reactions. Thus, a material having a higher reaction rate towards the degradation of organic compounds when compared to another material, will result in it having a higher bacterial degradation rate. The anti-bacterial activity of the three materials is presented in Fig. 16.

The as-produced TiO_2NT-EG array has an exceedingly high anti-bacterial rate with a reduction of 93.4% of the *E.Coli* population. The loss in the reaction rate towards *E.Coli* over 12 weeks aging is of just 13.4%. This value is lower than the loss in activity towards the degradation of MB after just one week of aging. There is a gradual small decline in activity, where the activity after one week of aging was 90.4% whereas that at the end of the aging exercise was 79.61%. There is also no evident stabilisation in the rate, with a slight reduction being observed at each timepoint. The increase in deposition of non-

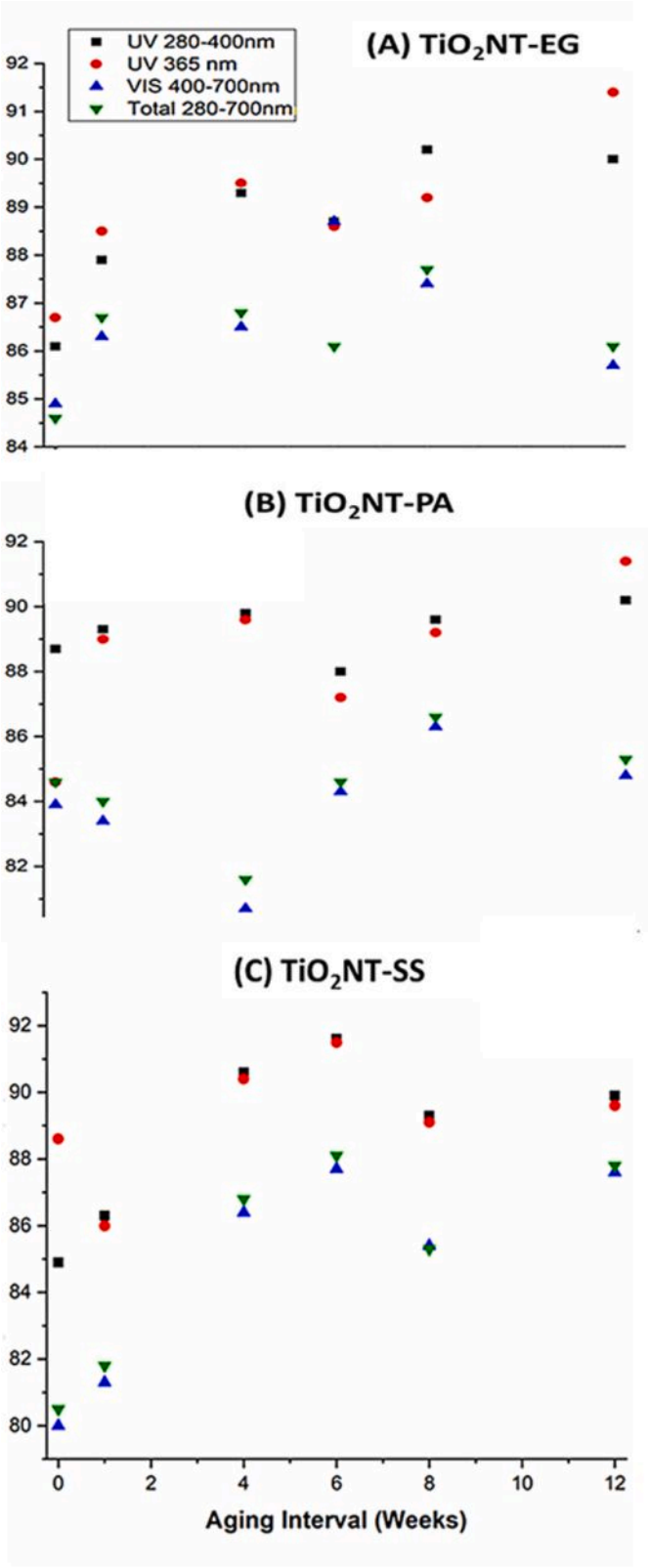

Fig. 11. Variation of spectral irradiance of the nanotube arrays during the aging regimen (a) TiO_2NT-EG (b) TiO_2NT-PA (c) TiO_2NT-SS.

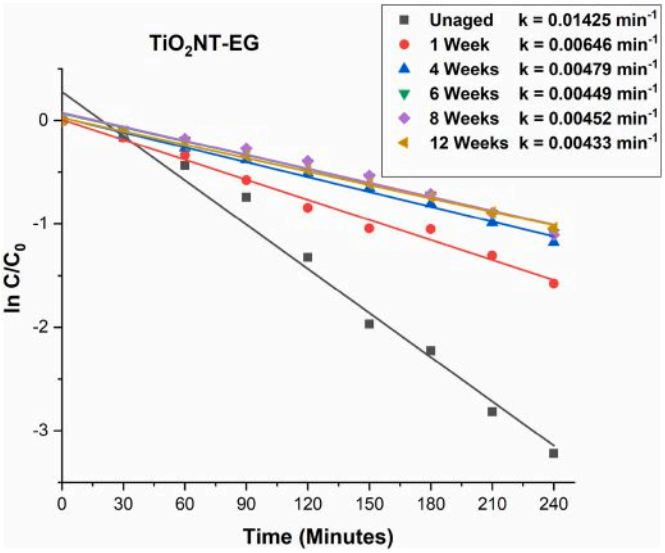

Fig. 12. Temporal variations in methylene blue degradation efficiencies over TiO_2NT-EG. (For interpretation of the references to colour in this figure legend, the reader is referred to the Web version of this article.)

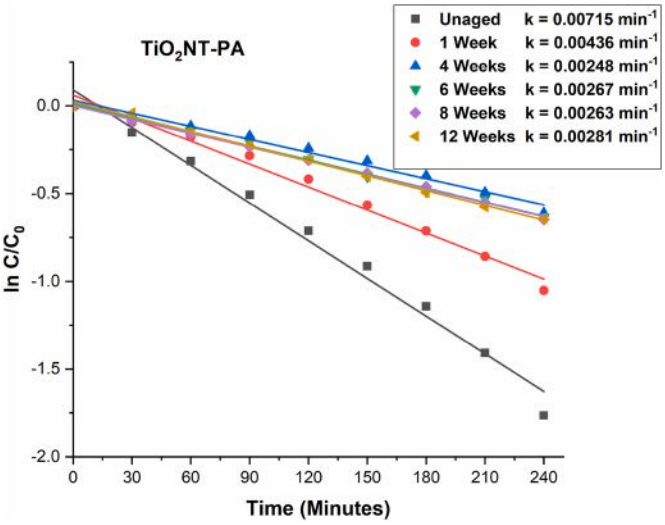

Fig. 13. Temporal variations in methylene blue degradation efficiencies over TiO_2NT-PA. (For interpretation of the references to colour in this figure legend, the reader is referred to the Web version of this article.)

photocatalytic material through the weekly loading with fresh synthetic greywater did not have the same detrimental effect as experienced with the MB results. The major effect of the salt layers and the other modes of fouling could have been simply to reduce the available surface area for the molecule to 'dock' onto the surface. Whilst the reduction of exposed surface might have hindered the production of ROS, oxidants which migrated through the debris layer could react with the bacteria found further from the surface. These results are very encouraging as they suggest that the aged surface can still retain a high level of its original activity. Thus, the possibility exists that on cleaning the surface sufficiently much of the activity is restored.

The antibacterial activity of the unaged TiO_2NT-PA nanotubes at 76.7% was markedly different than that of TiO_2NT-EG. This result agrees with the MB degradation rate also being lower. A gradual small reduction in activity to a value of 70.3% was obtained by the sixth week of aging. After the sixth week a more distinct change to 60.3% and 47.0% after the eighth and twelfth week of aging respectively was obtained. This indicates that whilst a certain degree of reduction in activity is inevitable with any degree of fouling, there is a certain amount of reduction in exposed surface area which results in a significant reduction in the rate of the photocatalytic reaction. The dense layer of debris

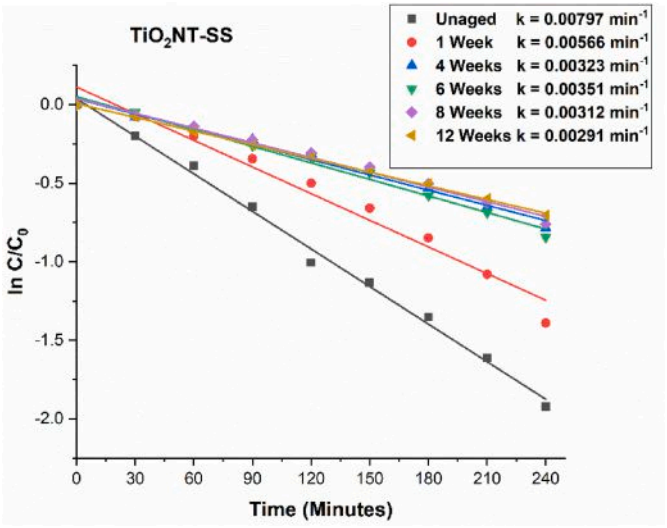

Fig. 14. Temporal variations in methylene blue degradation efficiencies over TiO_2NT-SS. (For interpretation of the references to colour in this figure legend, the reader is referred to the Web version of this article.)

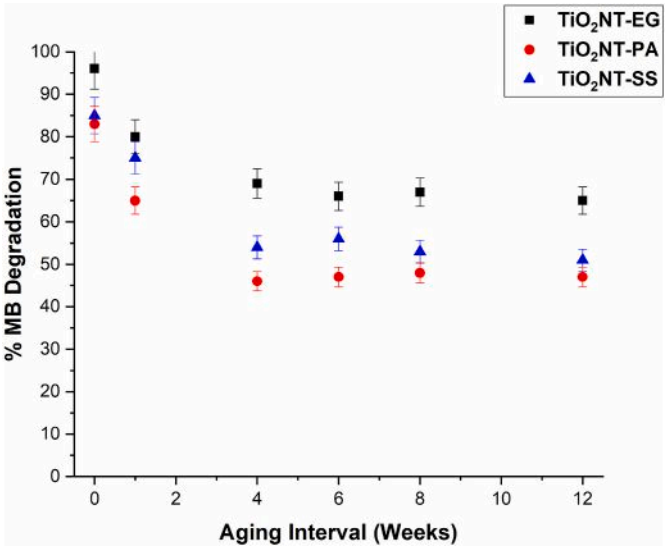

Fig. 15. Comparison of methylene blue degradation activities with aging. (For interpretation of the references to colour in this figure legend, the reader is referred to the Web version of this article.)

on the surface can trap or react with the ROS efficiently, making diffusion of the oxidising species more difficult, resulting a lower number of oxidants being available for the intended reaction. Similarly, the black organic residue can react with the available oxidisers which lowers the amount being available to interact with the cells.

The activity level of TiO_2NT-SS at 79.00% is close to that of TiO_2NT-PA and mirrors the results of the MB degradation test. The change in activity with aging also followed that of TiO_2NT-PA with the first major decline in activity occurring after eight weeks of aging, denoted by a value of 65.33%. The final activity at the end of the aging cycle was 45.29%. The reduction in activity can be attributed to the same factors which affected the TiO_2NT-PA surface. The deposition of inorganic debris coupled with the narrower tube tops severely compromised the activity of the material, despite its thickness being nearly double that of TiO_2NT-PA.

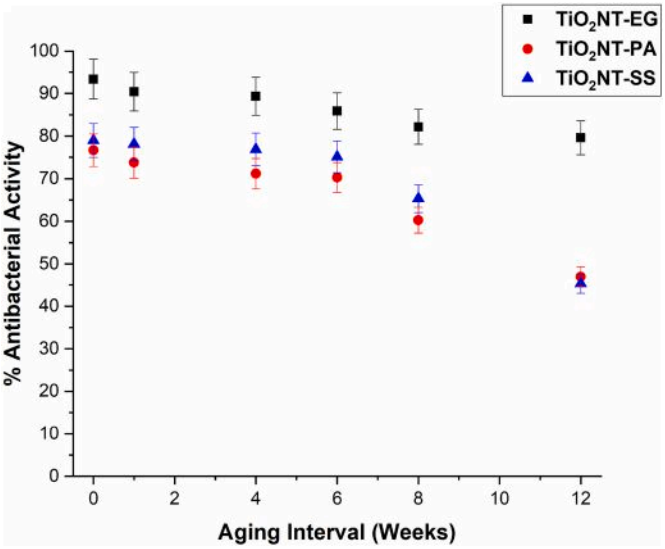

Fig. 16. Change in antibacterial activity with aging of the photocatalyst.

4. Conclusion

The mechanical stability and photocatalytic activity after twelve weeks aging of the three nanotube arrays synthesised in different electrolytes was assessed. The materials were all resistant to detachment and photo-induced corrosion and had a stable anatase crystalline phase. The morphology of the different arrays affected their resistance to fouling with the closely packed tubes in TiO_2NT-EG having the cleaner surface at the end of the aging exercise. The wider and well separated tubes in TiO_2NT-PA were extremely prone to the deposition of insoluble material over the photocatalyst surface. The well-separated but narrower nanotubes in TiO_2NT-SS also provided a degree of protection from fouling. A significant level of photocatalytic activity was sustained despite the repetitive photocatalytic activation and weekly loading with more insoluble materials. The activity of TiO_2NT-EG towards the degradation of methylene blue and the antibacterial effect on *E.Coli* remained the highest at the end of the aging cycle. The antibacterial activities of TiO_2NT-PA and TiO_2NT-SS at the end of the twelve-week experiment were nearly identical whilst TiO_2NT-SS retained a slightly higher methylene blue degradation rate. These results indicate that TiO_2 nanotubes with different morphologies can be used in greywater reactors without laborious maintenance procedures. The increase in UV absorbance as material deposited on the surface did not enhance the activity. The debris could act as UV absorbers rather than conductors to the underlying material. The presence of particles on the surface could also stifle the photocatalytic reaction by providing a physical barrier towards the pollutant and also serve to degrade the ROS prior to reacting. The possibility to reactivate the surface through periodic cleaning might bolster the potential use of TiO_2NT-SS over TiO_2NT-EG. The organic electrolyte is more expensive and requires specialised treatment prior to disposal. The lower activity of TiO_2NT-SS can be corrected for by controlling process parameters such as the retention time. The ideal synthetic method must be determined through a thorough lifecycle costing and upscaling exercise.

Funding

This work is part of the project Micro Wastewater Treatment Systems using Photocatalytic Surfaces (Micro WatTS) – Project C1-1.1-70, co-financed by the European Regional Development Fund (ERDF) - INTERREG V. A. Italia-Malta.

Declaration of competing interest

The authors declare that they have no known competing financial interests or personal relationships that could have appeared to influence the work reported in this paper.

Appendix A. Supplementary data

Supplementary data to this article can be found online at https://doi.org/10.1016/j.matchemphys.2021.124986.

References

[1] A. Fujishima, K. Honda, Electrochemical photolysis of water at a semiconductor electrode, Nature 238 (1972) 37–38, 1972/07/01.
[2] K. Nakata, A. Fujishima, TiO2 photocatalysis: design and applications, J. Photochem. Photobiol. C Photochem. Rev. 13 (2012) 169–189, 2012/09/01/.
[3] H. Dong, G. Zeng, L. Tang, C. Fan, C. Zhang, X. He, et al., An overview on limitations of TiO2-based particles for photocatalytic degradation of organic pollutants and the corresponding countermeasures, Water Res. 79 (2015) 128–146, 2015/08/01/.
[4] S.-Y. Lee, S.-J. Park, TiO2 photocatalyst for water treatment applications, J. Ind. Eng. Chem. 19 (2013) 1761–1769, 2013/11/25/.
[5] X. Zhu, Y. Chang, Y. Chen, Toxicity and bioaccumulation of TiO2 nanoparticle aggregates in Daphnia magna, Chemosphere 78 (2010) 209–215, 2010/01/01/.
[6] L. Clément, C. Hurel, N. Marmier, Toxicity of TiO2 nanoparticles to cladocerans, algae, rotifers and plants – effects of size and crystalline structure, Chemosphere 90 (2013) 1083–1090, 2013/01/01/.
[7] R. Kaegi, A. Ulrich, B. Sinnet, R. Vonbank, A. Wichser, S. Zuleeg, et al., Synthetic TiO2 nanoparticle emission from exterior facades into the aquatic environment, Environ. Pollut. 156 (Nov 2008) 233–239.
[8] A. Al-Kattan, A. Wichser, R. Vonbank, S. Brunner, A. Ulrich, S. Zuin, et al., Release of TiO2 from paints containing pigment-TiO2 or nano-TiO2 by weathering, Environ. Sci. Process Impacts 15 (Dec 2013) 2186–2193.
[9] L. Reijnders, The release of TiO2 and SiO2 nanoparticles from nanocomposites, Polym. Degrad. Stabil. 94 (2009/05/01/2009) 873–876.
[10] R. Singh, S. Dutta, A review on H2 production through photocatalytic reactions using TiO2/TiO2-assisted catalysts, Fuel 220 (2018) 607–620, 05/15.
[11] Q. Dou, P. Shrotriya, W. Li, K.R. Hebert, Stress-generating electrochemical reactions during the initial growth of anodic titanium dioxide nanotube layers, Electrochim. Acta 295 (2019) 418–426, 2019/02/01/.
[12] S. Cao, W. Huang, L. Wu, M. Tian, Y. Song, On the interfacial adhesion between TiO2 nanotube Array layer and Ti substrate, Langmuir 34 (2018) 10–26.
[13] D. Yu, X. Zhu, Z. Xu, X. Zhong, Q. Gui, Y. Song, et al., Facile method to enhance the adhesion of TiO2 nanotube Arrays to Ti substrate, ACS Appl. Mater. Interfaces 6 (2014) 8001–8005, 2014/06/11.
[14] S. Cao, W. Huang, S. Zhang, L. Wu, Y. Song, A simple strategy to increase the interfacial adhesion between TiO2 nanotube layer and Ti substrate, J. Alloys Compd. 772 (2019) 173–177, 2019/01/25/.
[15] N. Yao, K. Lun Yeung, Investigation of the performance of TiO2 photocatalytic coatings, Chem. Eng. J. 167 (2011) 13–21, 2011/02/15/.
[16] J. Olabarrieta, S. Zorita, I. Peña, N. Rioja, O. Monzón, P. Benguria, et al., Aging of photocatalytic coatings under a water flow: long run performance and TiO2 nanoparticles release, Appl. Catal. B Environ. 123–124 (2012) 182–192, 2012/07/23.
[17] D. Wang, L. Liu, F. Zhang, K. Tao, E. Pippel, K. Domen, Spontaneous phase and morphology transformations of anodized titania nanotubes induced by water at room temperature, Nano Lett. 11 (2011) 3649–3655, 2011/09/14.
[18] C. Cao, J. Yan, Y. Zhang, L. Zhao, Stability of titania nanotube arrays in aqueous environment and the related factors, Sci. Rep. 6 (2016) 23065, 2016/03/10.
[19] N. Liu, S.P. Albu, K. Lee, S. So, P. Schmuki, Water annealing and other low temperature treatments of anodic TiO2 nanotubes: a comparison of properties and efficiencies in dye sensitized solar cells and for water splitting, Electrochim. Acta 82 (2012) 98–102, 2012/11/01/.
[20] M. Assefpour-Dezfuly, C. Vlachos, E.H. Andrews, Oxide morphology and adhesive bonding on titanium surfaces, J. Mater. Sci. 19 (1984) 3626–3639, 1984/11/01.
[21] V. Zwilling, M. Aucouturier, E. Darque-Ceretti, Anodic oxidation of titanium and TA6V alloy in chromic media. An electrochemical approach, Electrochim. Acta 45 (1999) 921–929, 1999/12/01/.
[22] J.M. Macak, M. Zlamal, J. Krysa, P. Schmuki, Self-Organized TiO2 nanotube layers as highly efficient photocatalysts, Small 3 (2007) 300–304.
[23] A. Ghicov, J.M. Macak, H. Tsuchiya, J. Kunze, V. Haeublein, L. Frey, et al., Ion implantation and annealing for an efficient N-doping of TiO2 nanotubes, Nano Lett. 6 (2006) 1080–1082, 2006/05/01.
[24] I. Paramasivam, J.M. Macak, P. Schmuki, Photocatalytic activity of TiO2 nanotube layers loaded with Ag and Au nanoparticles, Electrochem. Commun. 10 (2008) 71–75, 2008/01/01/.
[25] J.R. Jennings, A. Ghicov, L.M. Peter, P. Schmuki, A.B. Walker, Dye-Sensitized solar cells based on oriented TiO2 nanotube Arrays: transport, trapping, and transfer of electrons, J. Am. Chem. Soc. 130 (2008) 13364–13372, 2008/10/08.
[26] A. El Ruby Mohamed, S. Rohani, Modified TiO2 nanotube arrays (TNTAs): progressive strategies towards visible light responsive photoanode, a review, Energy Environ. Sci. 4 (2011) 1065–1086.
[27] S. Bauer, S. Kleber, P. Schmuki, TiO2 nanotubes: tailoring the geometry in H3PO4/HF electrolytes, Electrochem. Commun. 8 (2006) 1321–1325, 2006/08/01/.
[28] C. Ruan, M. Paulose, O.K. Varghese, C.A. Grimes, Enhanced photoelectrochemical-response in highly ordered TiO2 nanotube-arrays anodized in boric acid containing electrolyte, Sol. Energy Mater. Sol. Cell. 90 (2006) 1283–1295, 2006/05/23/.
[29] M. Paulose, K. Shankar, S. Yoriya, H.E. Prakasam, O.K. Varghese, G.K. Mor, et al., Anodic growth of highly ordered TiO2 nanotube Arrays to 134 μm in length, J. Phys. Chem. B 110 (2006) 16179–16184, 2006/08/01.
[30] S. Kaneco, Y. Chen, P. Westerhoff, J.C. Crittenden, Fabrication of uniform size titanium oxide nanotubes: impact of current density and solution conditions, Scripta Mater. 56 (2007) 373–376, 2007/03/01/.
[31] H.E. Prakasam, K. Shankar, M. Paulose, O.K. Varghese, C.A. Grimes, A new benchmark for TiO2 nanotube Array growth by anodization, J. Phys. Chem. C 111 (2007) 7235–7241, 2007/05/01.
[32] H. Xu, S. Ouyang, L. Liu, P. Reunchan, N. Umezawa, J. Ye, Recent advances in TiO2-based photocatalysis, J. Mater. Chem. 2 (2014) 12642–12661.
[33] J.B. Kerr, V.E. Fioletov, Surface ultraviolet radiation, Atmos.-Ocean 46 (2008) 159–184, 2008/01/01.
[34] A. Cabrera-Reina, A.B. Martínez-Piernas, Y. Bertakis, N.P. Xekoukoulotakis, A. Agüera, J.A. Sánchez Pérez, TiO2 photocatalysis under natural solar radiation for the degradation of the carbapenem antibiotics imipenem and meropenem in aqueous solutions at pilot plant scale, Water Res. 166 (2019) 115037, 2019/12/01/.
[35] J. Shi, W. Huang, H. Zhu, J. Xiong, H. Bei, X. Wei, et al., Modified TiO2 particles for heterogeneous photocatalysis under solar irradiation, Mater. Lett. 279 (2020) 128472, 2020/11/15/.
[36] K. Thompson, R. Summers, S. Cook, Development and experimental validation of the composition and treatability of a new synthetic bathroom greywater (SynGrey), Environ. Sci.: Water Res. Technol. 3 (2017), 09/15.
[37] ASTM, G173-03, Standard Tables for Reference Solar Spectral Irradiances: Direct Normal and Hemispherical on 37 Tilted Surface, ASTM International, West Conshohocken, PA, 2012.
[38] C.F.F. Lia, M.A. Buccheri, G. Rappazzo, E. Zammit, A. Rizzo, M. Grech, P. Refalo, S. Abela, Effect of the surface morphology of TiO2 nanotubes on photocatalytic efficacy using electron-transfer-based assays and antimicrobial tests, Appl. Sci. 10 (15) (2020) 5243.
[39] I. O. f. Standardisation, Fine ceramics (advanced ceramics, advanced technical ceramics) — Determination of photocatalytic activity of surfaces in an aqueous medium by degradation of methylene blue, 1st, ISO 10678, 2010.
[40] R. Wang, K. Hashimoto, A. Fujishima, M. Chikuni, E. Kojima, A. Kitamura, et al., Light-induced amphiphilic surfaces, Nature 388 (1997) 431–432, 1997/07/01.
[41] X. Zhou, N.T. Nguyen, S. Özkan, P. Schmuki, Anodic TiO2 nanotube layers: why does self-organized growth occur—a mini review, Electrochem. Commun. 46 (2014) 157–162, 2014/09/01/.
[42] H. Habazaki, K. Fushimi, K. Shimizu, P. Skeldon, G.E. Thompson, Fast migration of fluoride ions in growing anodic titanium oxide, Electrochem. Commun. 9 (2007) 1222–1227, 2007/05/01/.
[43] S. Berger, S. Albu, F. Schmidt-Stein, H. Hildebrand, P. Schmuki, J. Hammond, et al., The origin for tubular growth of TiO2 nanotubes: a fluoride rich layer between tube-walls, Surf. Sci. 605 (2011), 10/01.
[44] M.C. Hidalgo, D. Bahnemann, Highly photoactive supported TiO2 prepared by thermal hydrolysis of TiOSO4: optimisation of the method and comparison with other synthetic routes, Appl. Catal. B Environ. 61 (2005) 259–266, 2005/11/09/.
[45] G.E. Christidis, Industrial Clays 9 (2011) 341–414.
[46] K. Fischer, M. Kühnert, R. Gläser, A. Schulze, Photocatalytic degradation and toxicity evaluation of diclofenac by nanotubular titanium dioxide–PES membrane in a static and continuous setup, RSC Adv. 5 (2015) 16340–16348.
[47] J. Zhang, P. Zhou, J. Liu, J. Yu, New understanding of the difference of photocatalytic activity among anatase, rutile and brookite TiO2, Phys. Chem. Chem. Phys. 16 (2014) 20382–20386.
[48] A. Ghicov, H. Tsuchiya, J.M. Macak, P. Schmuki, Annealing effects on the photoresponse of TiO2 nanotubes, Phys. Status Solidi 203 (2006) R28–R30.
[49] X. Yan, Y. Li, T. Xia, Black titanium dioxide nanomaterials in photocatalysis, Int. J. Photoenergy (2017) 8529851, 2017/11/02.
[50] D.A.H. Hanaor, C.C. Sorrell, Review of the anatase to rutile phase transformation, J. Mater. Sci. 46 (2011) 855–874, 2011/02/01.
[51] S. Koneshan, J.C. Rasaiah, R.M. Lynden-Bell, S.H. Lee, Solvent structure, dynamics, and ion mobility in aqueous solutions at 25 °C, J. Phys. Chem. B 102 (1998) 4193–4204, 1998/05/01.
[52] P. Roy, S.P. Albu, P. Schmuki, TiO2 nanotubes in dye-sensitized solar cells: higher efficiencies by well-defined tube tops, Electrochem. Commun. 12 (2010) 949–951, 2010/07/01/.
[53] H. Liang, H. Han, F. Wang, Z. Cheng, B. Lin, Y. Pan, et al., Experimental investigation on spectral splitting of photovoltaic/thermal hybrid system with two-axis sun tracking based on SiO2/TiO2 interference thin film, Energy Convers. Manag. 188 (2019) 230–240, 2019/05/15/.
[54] C. Farrugia, A. Di Mauro, F. Lia, E. Zammit, A. Rizzo, V. Privitera, et al., Suitability of different titanium dioxide nanotube morphologies for photocatalytic water treatment, Nanomaterials 11 (2021) 708.
[55] H.Y. Chen, O. Zahraa, M. Bouchy, Inhibition of the adsorption and photocatalytic degradation of an organic contaminant in an aqueous suspension of TiO2 by inorganic ions, J. Photochem. Photobiol. Chem. 108 (1997) 37–44, 1997/07/31/.

[56] D. Awfa, M. Ateia, M. Fujii, C. Yoshimura, Photocatalytic degradation of organic micropollutants: inhibition mechanisms by different fractions of natural organic matter, Water Res. 174 (2020) 115643, 2020/05/01/.
[57] C.S. Turchi, D.F. Ollis, Mixed reactant photocatalysis: intermediates and mutual rate inhibition, J. Catal. 119 (1989) 483–496, 1989/10/01/.
[58] S.D. Snow, C.E.L. LaRoy, V.V. Tarabara, Photocatalysis in membrane bioreactor effluent: assessment of inhibition by dissolved organics, J. Environ. Eng. 145 (2019), 06019001.
[59] M. Abdullah, G.K.C. Low, R.W. Matthews, Effects of common inorganic anions on rates of photocatalytic oxidation of organic carbon over illuminated titanium dioxide, J. Phys. Chem. 94 (1990) 6820–6825, 1990/08/01.
[60] M. Lindner, D.W. Bahnemann, B. Hirthe, W.-D. Griebler, Solar water detoxification: novel TiO2 powders as highly active photocatalysts, J. Sol. Energy Eng. 119 (1997) 120–125.
[61] W. Zhang, T. An, M. Cui, G. Sheng, J. Fu, Effects of anions on the photocatalytic and photoelectrocatalytic degradation of reactive dye in a packed-bed reactor, J. Chem. Technol. Biotechnol. 80 (2005) 223–229.
[62] C. Guillard, E. Puzenat, H. Lachheb, A. Houas, J.-M. Herrmann, Why inorganic salts decrease the TiO2 photocatalytic efficiency, Int. J. Photoenergy 7 (2005) 641208, 1900/01/01.
[63] S.W. Karickhoff, G.W. Bailey, Optical absorption spectra of clay minerals, Clay Clay Miner. 21 (1973) 59–70, 1973/02/01.
[64] W. Wang, G. Huang, J.C. Yu, P.K. Wong, Advances in photocatalytic disinfection of bacteria: development of photocatalysts and mechanisms, J. Environ. Sci. 34 (2015) 232–247, 2015/08/01/.